DOI: 10.1002/ejic.200600380

Synthesis of a New Tetrakis(2-pyridinyl)pyrazine Complex of Gold(III) and Its Computational, Spectroscopic and Electrochemical Characterization

Marco Bortoluzzi,*[a] Eddy De Faveri,[b] Salvatore Daniele,[b] and Bruno Pitteri[a]

Keywords: Gold / N ligands / Density functional calculations / Electrochemistry

The cationic dinuclear (hydroxo)Au^{III} complex $[Au_2(OH)_2(tppz)]Cl_4$ [tppz = 2,3,5,6-tetrakis(2-pyridinyl)pyrazine] was prepared by allowing the ligand tppz to react with $K[AuCl_4]\cdot 2H_2O$ in refluxing methanol. Its NMR and IR spectra support the formation of a symmetric hydroxo derivative instead of the expected chloro complex. DFT B3PW91 calculations were performed with various basis sets to give better insights into the properties of the prepared complex and to compare it with the known derivative $[Au(OH)(terpy)]^{2+}$ (terpy = 2,2′:6′,2′′-terpyridine). The electrochemical behaviour of $[Au_2(OH)_2(tppz)]Cl_4$ was investigated by cyclic voltammetry and it was found that two main irreversible reduction processes occurred. In particular, a four-electron process, leading to the formation of gold(I) complex species in solution, and a two-electron process affording metallic gold were observed. The electronicity involved in the two processes was verified by macroelectrolysis at controlled potential.

Introduction

Pyridine-derived polydentate ligands play a fundamental role in inorganic chemistry and one of the most interesting molecules of this kind is the terdentate ligand 2,2′:6′,2′′-terpyridine (terpy; Scheme 1), whose coordination chemistry with Au^{III} has been studied in the past few years. In particular, chloro- and hydroxogold(III)–terpy complexes of the type $[AuL(terpy)]^{2+}$ (L = Cl, OH) are known that have been structurally characterized.[1,2] In the field of gold complexes with pyridine-based polydentate ligands, much less attention has been devoted to the ligand 2,3,5,6-tetrakis(2-pyridinyl)pyrazine (tppz; Scheme 1), even though it can be approximately considered as a "double terpyridine" and, therefore, is suited to coordinate two metal fragments to form complexes having a strong electronic delocalization.

A number of tppz complexes of transition metals such as ruthenium and osmium,[3] iron,[4] rhodium,[5] iridium,[6] nickel,[7] palladium,[8] copper[7,9,10] and zinc[10] have been prepared, whereas, to the best of our knowledge, no example of a gold derivative of 2,3,5,6-tetrakis(2-pyridinyl)pyrazine has been published in the literature. The previous works regarding tetrakis(2-pyridinyl)pyrazine coordination chemistry demonstrated that both mono- and dinuclear tppz complexes can be synthesized and that it is also possible to obtain mixed-metal tppz derivatives. Many of these tetrakis(2-pyridinyl)pyrazine complexes have shown intriguing spectroelectrochemical and electrochemical properties due to the characteristics of the tppz ligand.

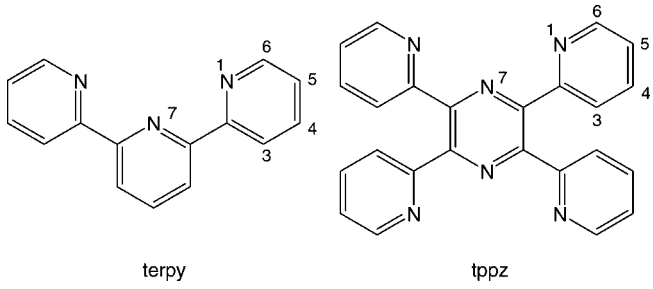

Scheme 1. 2,2′:6′,2′′-Terpyridine (terpy) and 2,3,5,6-tetrakis(2-pyridinyl)pyrazine (tppz) and the numbering of their hydrogen and nitrogen atoms.

In this paper the synthesis of a tetrakis(2-pyridinyl)pyrazine derivative of gold, the dinuclear hydroxo complex $[Au_2(OH)_2(tppz)]Cl_4$, is reported for the first time. DFT B3PW91 calculations are also performed to give better insights into the electronic and steric properties of the prepared compound and to compare it with the known $[Au(OH)(terpy)]^{2+}$ cation. Cyclic voltammetric experiments and macroelectrolysis at controlled potential are performed to understand the redox properties of $[Au_2(OH)_2(tppz)]Cl_4$ and to ascertain an eventual formation of stable tetrakis(2-pyridinyl)pyrazine derivatives of gold(I) in solution.

Results and Discussion

Preparation and Characterization of the Complex

The hydroxo complex $[Au_2(OH)_2(tppz)]Cl_4$ was prepared by treating the ligand 2,3,5,6-tetrakis(2-pyridinyl)pyrazine

[a] Dipartimento di Chimica, Università Ca' Foscari di Venezia, Dorsoduro 2137, 30123 Venezia, Italy
E-mail: markos@unive.it
[b] Dipartimento di Chimica Fisica, Università Ca' Foscari di Venezia, Dorsoduro 2137, 30123 Venezia, Italy

(tppz) with potassium tetrachloroaurate dihydrate $K[AuCl_4]\cdot 2H_2O$ in refluxing methanol (see Scheme 2). On the basis of previous works with the terpy ligand,[1,2] the formation of the chloro complex $[Au_2Cl_2(tppz)]^{2+}$ was expected. However, both the IR and the ^1H NMR spectra of the reaction product support the presence of a coordinated hydroxo ligand. Thus, an O–H stretching is observable in the IR spectrum (3412 cm^{-1}) and the hydrogen atoms of the OH ligands give a broad signal in the ^1H NMR spectrum. The chemical shift of this signal is, as expected, quite dependent upon the temperature. The formation of a hydroxo ligand is probably due to the presence of water in the reaction mixture coming from the starting precursor $K[AuCl_4]\cdot 2H_2O$. All the pyridine rings are magnetically equivalent, and only four signals attributable to coordinated tppz can be observed in the ^1H NMR spectrum. Also, the $^{13}C\{^1H\}$ NMR spectrum shows signals of only four primary carbon atoms and two quaternary carbon atoms. This means that the prepared compound is dinuclear and that both the gold atoms have the same coordination environment. Finally, the elemental analyses (C, H, Cl, N) are also in agreement with the proposed formulation, the deviations between found and calculated values being less than 0.4%.

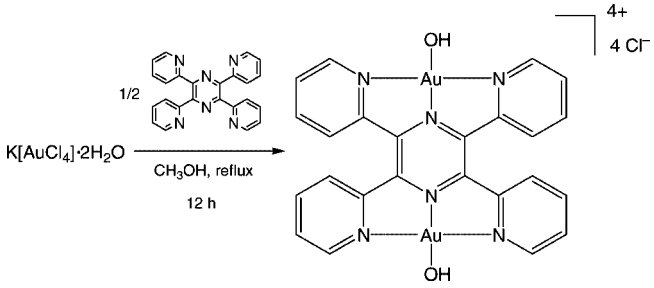

Scheme 2. Synthesis of $[Au_2(OH)_2(tppz)]Cl_4$.

DFT Studies

To better understand the electronic and steric properties of the prepared compound, computational geometry optimisations of the cations $[Au(OH)(terpy)]^{2+}$ and $[Au_2(OH)_2(tppz)]^{4+}$ were performed using the DFT B3PW91 method. Table 1 shows the r_{Au-O}, r_{Au-N7} and the average r_{Au-N1} bond lengths of $[Au(OH)(terpy)]^{2+}$ and $[Au_2(OH)_2(tppz)]^{4+}$. The average C6–N1–Au–O dihedral angle and the Mulliken charge of the coordinated [AuOH] fragments are also included. The differences between the DFT-calculated bond lengths and the bond lengths found in the X-ray structure analysis of $[Au(terpy)(OH)](ClO_4)_2$[2] are always less than 2.2%; the greatest deviation between calculated and experimental r_{Au-O} bond lengths is less than 1.2%.

The average r_{Au-N1} and r_{Au-O} bond lengths for both optimised cations are almost identical to within three significant figures, whereas the Au–N7 bond in the $[Au_2(OH)_2(tppz)]^{4+}$ complex is about 0.03 Å longer than that in the monomer. The coordination of two gold fragments strongly twists the molecule from planarity because of the steric hindrance between the H3 atoms of the pyridine rings. The degree of twisting can be quantified by comparing the C6–N1–Au–O dihedral angles of $[Au(OH)(terpy)]^{2+}$ and $[Au_2(OH)_2(tppz)]^{4+}$: the terpy derivative is approximately planar, with an average C6–N1–Au–O dihedral angle of less than 1°, while the dinuclear [tetrakis(2-pyridinyl)pyrazine]gold derivative has an average C6–N1–Au–O dihedral angle of between 9.0° and 9.8°, depending upon the basis set. A similar deviation of the tetrakis(2-pyridinyl)pyrazine ligand from planarity has already been observed in the X-ray structures of dinuclear tppz derivatives of various transition metals.[3,5–10]

From the calculated geometries, a C_{2h} symmetry can be ascribed to the $[Au_2(OH)_2(tppz)]^{4+}$ cation, which is in agreement with the corresponding ^1H NMR and $^{13}C\{^1H\}$ NMR spectra. The DFT B3LYP/BS3 optimised geometry of $[Au_2(OH)_2(tppz)]^{4+}$ is shown in Figure 1.

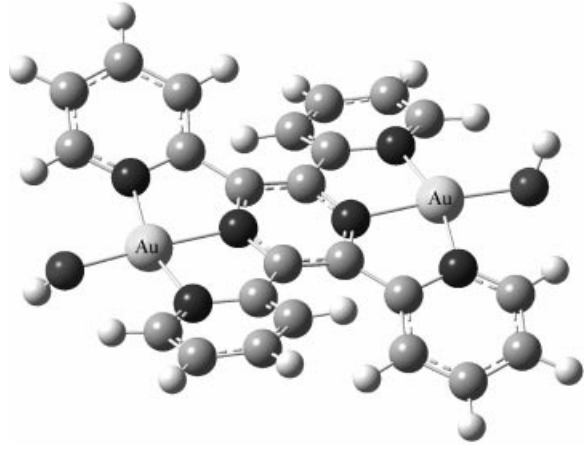

Figure 1. DFT B3LYP/BS3 optimised geometry of the $[Au_2(OH)_2(tppz)]^{4+}$ cation.

Table 1. Selected bond lengths and angles for the cations $[Au(OH)(terpy)]^{2+}$ and $[Au_2(OH)_2(tppz)]^{4+}$ and the Mulliken charge of the coordinated [AuOH] fragment. **BS1**: CEP-121G, CEP-31G on Au; **BS2**: D95V, SDD on Au; **BS3**: D95, LANL2DZ on Au.

Complex	r_{Au-N1} [Å]	r_{Au-N7} [Å]	r_{Au-O} [Å]	C6–N1–Au–O [°]	[AuOH] charge
BS1					
$[Au(OH)(terpy)]^{2+}$	2.0484	1.9916	1.9796	0.4	0.786
$[Au_2(OH)_2(tppz)]^{4+}$	2.0421	2.0224	1.9646	9.4	0.891
BS2					
$[Au(OH)(terpy)]^{2+}$	2.0370	1.9871	1.9897	0.6	0.886
$[Au_2(OH)_2(tppz)]^{4+}$	2.0312	2.0194	1.9764	9.0	0.953
BS3					
$[Au(OH)(terpy)]^{2+}$	2.0423	1.9855	1.9763	0.9	0.831
$[Au_2(OH)_2(tppz)]^{4+}$	2.0377	2.0151	1.9597	9.8	0.915

The Mulliken charge of the [AuOH] fragments in the $[Au_2(OH)_2(tppz)]^{4+}$ cation is always higher than that calculated for the $[Au(OH)(terpy)]^{2+}$ complex (see Table 1). This means that the tetrakis(2-pyridinyl)pyrazine derivative has less basic hydroxo ligands and more electrophilic gold centres and this fact can be ascribed to the lower ability of the tppz ligand, if compared with two terpy molecules, to delocalize the positive charge on its aromatic rings. The mechanism of formation of the mononuclear $[Au(OH)(terpy)]^{2+}$ cation from the chloro complex $[AuCl(terpy)]^{2+}$ and the equilibrium between this hydroxo derivative and the corresponding aqua complex $[Au(OH_2)(terpy)]^{3+}$ has been studied in a previous paper.[2] It was found that the water molecule coordinated to the $[Au(terpy)]^{3+}$ fragment behaves as a strong acid ($K_a \geq 0.8$ M). It therefore seems reasonable to hypothesise that the mechanism leading to the $[Au_2(OH)_2(tppz)]Cl_4$ complex could be similar to that of the analogous terpy derivative. Thus, the reaction between tppz and $AuCl_4^-$ probably leads to the initial formation of an intermediate chloro species. This may react with water present in the reaction medium to give a very acidic aqua species which, on the basis of the DFT calculations, would be even more acidic than the corresponding $[Au(OH_2)(terpy)]^{3+}$ complex and, consequently, would deprotonate to provide the final $[Au_2(OH)_2(tppz)]Cl_4$ hydroxo species. It must be considered that, although the formation of (aqua)-Au^{III}–tppz derivatives is disfavoured by the experimental conditions, the driving force of the whole reaction is the immediate deprotonation of the coordinated water molecules. The $[Au_2(OH)_2(tppz)]Cl_4$ product should be very stable as the square-planar hydroxo species is known to be inert towards nucleophilic substitution.[11] Besides, the very similar values of the calculated r_{Au-O} bond lengths in $[Au_2(OH)_2(tppz)]^{4+}$ and $[Au(OH)(terpy)]^{2+}$ (see Table 1) and the fact that the terpy derivative is rather stable allowed us to conclude that the same lack of reactivity occurs for the dinuclear Au^{III} complex prepared in this work.

On the other hand, because the formation of a 6+ diaquo intermediate of the type $[Au_2(OH_2)_2(tppz)]^{6+}$ in solution is rather improbable as its acidity should be even higher than that of a 5+ aquo species like $[Au_2Cl(OH_2)(tppz)]^{5+}$ or $[Au_2(OH)(OH_2)(tppz)]^{5+}$, a possible reaction pathway leading to the hydroxo derivative from the intermediate chloro species is that summarized in Scheme 3.

Electrochemical Characterisation

The redox properties of $[Au_2(OH)_2(tppz)]Cl_4$ were investigated by cyclic voltammetry (CV) with both conventional and microelectrodes.[13,14] Figure 2 shows a typical cyclic voltammogram recorded for $[Au_2(OH)_2(tppz)]Cl_4$ at 50 mV s^{-1} with a 3 mm glassy carbon electrode, displaying a rather complex pattern. In particular, in the forward scan, two main irreversible cathodic processes occurring at –0.030 and –0.70 V (**A** and **B**, respectively, in Figure 2), and a series of smaller processes, which occur over the potential region from –1.5 to –2.2 V, are observed. In the reverse scan, apart from the small peaks associated with the latter processes, two major peaks, occurring at 0.56 and 1.16 V (**C** and **D**, respectively, in Figure 2), are observed. Direct anodic scans, starting from 0.3 V, also displayed peak **D**, which is characterised by its much smaller height (see Figure 2 dashed line). This finding suggests that a bulk solution species is responsible for the latter electrode process. Voltammetric measurements performed in DMF solutions containing the supporting electrolyte and increasing amounts of $[BzEt_3N]Cl$ allowed us to assign peak **D** as being due to the oxidation of free Cl^- ions. Similarly, the series of small cathodic and anodic patterns over the potential region from –1.5 to –2.2 V were assigned to an electrode process involving free tppz ligand, as checked in solutions of pure sample. Peaks **A** and **B** probably involve the metal centres and our attention was therefore mainly devoted to these processes. It should be noted that peak **B** is rather broad, and a closer examination of its shape suggests that at least two overlapping peaks are present in it.

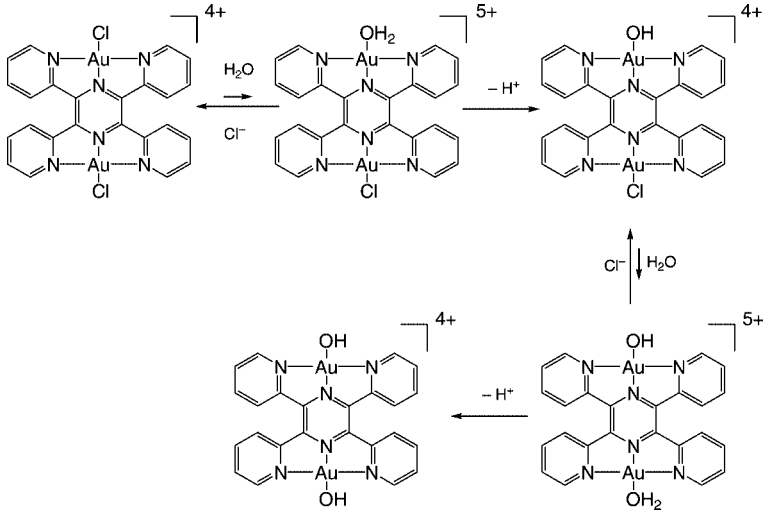

Scheme 3. Mechanism of formation of the $[Au_2(OH)_2(tppz)]Cl_4$ complex.

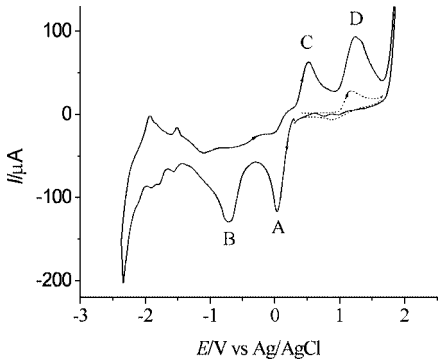

Figure 2. Cyclic voltammograms of 2 mM $[Au(OH)_2(tppz)]Cl_4$ in DMF + 0.1 M TBAP; (—) direct cathodic scan, (- - -) direct anodic scan. Glassy carbon electrode (3 mm diameter); scan rate: 50 mV s^{-1}.

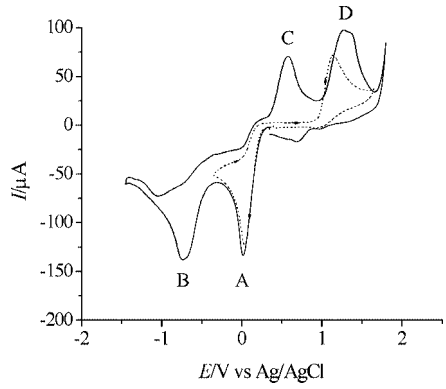

Figure 3. Cyclic voltammograms of 2 mM $[Au(OH)_2(tppz)]Cl_4$ in DMF + 0.1 M TBAP; (—) reversal of the scan direction after peak **B**, (- - -) reversal of the scan direction after peak **A**. Glassy carbon electrode (3 mm diameter); scan rate: 50 mV s^{-1}.

Figure 3 shows the cyclic voltammograms obtained for the $[Au_2(OH)_2(tppz)]Cl_4$ solution on reversal of the scan direction soon after either peak **A** or **B** were traversed. It is evident that peak **C** originates from the second cathodic process, while peak **D** increases strongly in current height after peak **A** has been traversed. This current increase indicates that a larger amount of Cl^- ions is formed at the electrode surface following the first reduction process. This circumstance, along with the conductivity value found for a 10^{-3} M $[Au_2(OH)_2(tppz)]Cl_4$ solution in DMF at 25 °C (Λ_M = 159 Ω^{-1} mol^{-1} cm^2), which is lower than that expected for a 4:1 electrolyte (i.e. in the range 250–300 Ω^{-1} mol^{-1} cm^2[12]), suggests that the $[Au_2(OH)_2(tppz)]^{4+}$ cation forms relatively stable ionic couples with chloride ions in DMF. Evidence for association of cationic gold(III) complexes of the type $[AuCl_2(N–N)]^+$ (N–N = sp^2-nitrogen-donating chelate ligands like 2,2′-bipyridine and 1,10-phenanthroline) with chloride in solution is known in the literature;[17] therefore, both the low conductivity value and the growth of peak **D** after the first reduction process were not unexpected. The above scenario did not change when performing cyclic voltammetric measurements at different scan rates over the range 0.01–0.5 V s^{-1}. The analysis of peak current (I_p) as a function of the square root of scan rate ($v^{1/2}$) was linear for both peaks **A** and **B**, thus indicating that they are diffusion-controlled processes.[13] An analysis of the peak potential (E_p) and the half-peak potential ($E_p - E_{p/2}$) ($E_{p/2}$ is the potential at $I_p/2$) as a function of scan rate over the above range was also performed. However, because of the complex nature of peak **B**, only the characteristics of peak **A** were examined from a quantitative point of view. It was found that $E_{p(A)}$ shifts by about 90 mV towards more negative potentials with a tenfold change of scan rate, although ($E_{p(A)} - E_{p/2}$) is equal to 106(±7) mV regardless of the scan rate. These findings are consisent with the occurrence of an irreversible electrode process.[13] The irreversible character of process **A** was further confirmed by CV measurements performed at higher scan rates with a platinum microdisk electrode. In fact, no oxidation process was directly associated to peak **A**, even when performing CV measurements at scan rates up to 500 V s^{-1}.[13]

Cyclic voltammetric measurements with the microelectrodes were also performed at low scan rates, and Figure 4 shows a typical CV obtained at 20 mV s^{-1}. Under these conditions sigmoidal waves, which are typical for microelectrodes working under steady-state conditions, were obtained.[14] The number of both cathodic and anodic processes observed, and their positions, are identical to those obtained with the conventional electrode. The shape of the voltammogram either confirmed or gave additional information with respect to that obtained with the conventional electrode. In particular, the analysis of wave **A** in terms of the Tomes difference ($E_{1/4} - E_{3/4}$)[15] (i.e. the difference between the potentials recorded at 1/4 and 3/4 of the steady-state limiting current of the forward waves) gave a value of 81(±2) mV, which is considerably higher than the value of 56.5/n mV (n is the number of electrons) expected theoretically for a reversible process at 24 °C.[13] This confirms the irreversible character of process **A**. The CV pattern on reversal of the scan direction from the second cathodic wave displays a current cross-over to which wave **C** is associated (see Figure 4). This behaviour is typical for metal deposition and growth on the electrode surface.[16] Therefore, the formation of metallic gold is conceivably occurring over the reduction process of the second wave. Consequently, wave **C** could be assigned to the stripping of metallic gold from the electrode surface.

The involvement of metallic gold in the correspondence of peak **C** was verified by performing a series of measurements with a conventional gold electrode in DMF solutions containing TBAP and, in consecutive steps, $[BzEt_3N]Cl$ and the tppz ligand. It was observed that the anodization of the gold electrode in the presence of $[BzEt_3N]Cl$ provided the peak at 0.56 V (peak **C**), probably due to the formation of gold chloride species.

The number of electrons involved in the two cathodic processes **A** and **B** was evaluated by preparative macroelectrolysis at controlled potential.[13] Exhaustive reduction performed at –0.4 V (where only **A** is reduced) yielded a charge consumption corresponding to a total of four electrons per mol of $[Au_2(OH)_2(tppz)]Cl_4$, i.e. an overall two-electron

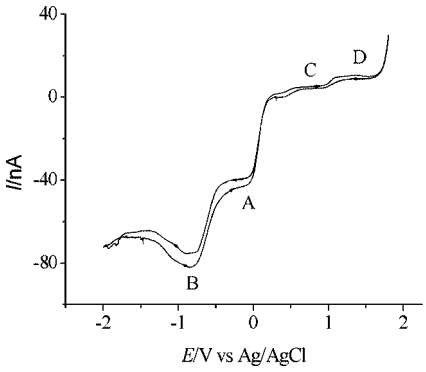

Figure 4. Cyclic voltammogram of 2 mM $[Au_2(OH)_2(tppz)]Cl_4$ in DMF + 0.1 M TBAP at a 12.5-μm Pt disk; scan rate: 20 mV s^{-1}.

process for each Au centre. During this experiment the solution turned from bright yellow to colourless. Cyclic voltammetric analysis of the electrolysed solution performed with a glassy carbon electrode displayed peak **B** in the cathodic scan and peaks **C** and **D** upon reversal of the scan direction. Only peak **D** was present in the direct anodic scan. It is also interesting to note that the voltammetric analysis performed on an electrolysed solution after a charge consumption corresponding to a an overall two electrons per mol of $[Au_2(OH)_2(tppz)]Cl_4$ still displays peak **A** with a height equal to half of its initial value, while peak **B** maintains almost the same height as in Figure 2. This suggests that the reduction of $[Au_2(OH)_2(tppz)]Cl_4$ provides only the species responsible for peak **B**, and that the electrons consumed are shared between the two Au^{III} centres, conceivably providing Au^{I} species.

Macroelectrolysis performed at –1.5 V (i.e. at peak **B**) required an overall two electrons per mol of the $[Au_2(OH)_2(tppz)]Cl_4$ complex, thus indicating a one-electron reduction process for each central atom. This reduction process affords metallic gold, as indicated by the fact that during electrolysis the platinum gauze becomes covered by a yellow film, conceivably due to a thick deposit of metallic gold,

Peak **A**

$$[Au^{III}_2(OH)_2(tppz)]Cl_4 \rightleftharpoons [Au_2(OH)_2(tppz)]Cl_{(4-i)}^{i+} + i\,Cl^-$$

$$[Au_2(OH)_2(tppz)]Cl_{(4-i)}^{i+} \xrightarrow{4\,e^-} Au_2(OH)_2(tppz) + (4-i)\,Cl^-$$

$$Au_2(OH)_2(tppz) \xrightarrow[fast]{} [Au_2(tppz)]^{2+} + 2\,OH^-$$

i = number of free Cl^-

Peak **B**

$$[Au_2(tppz)]^{2+} \xrightarrow{e^-} [Au_2(tppz)]^{+}$$

$$[Au_2(tppz)]^{+} \xrightarrow[fast]{} [Au(tppz)]^{+} + Au$$

$$[Au(tppz)]^{+} \xrightarrow{e^-} Au(tppz)$$

$$Au(tppz) \xrightarrow[fast]{} tppz + Au$$

Scheme 4. Reduction pathway at peaks **A** and **B**.

and at the same time the colour of the solution turned from almost colourless to yellow-orange. Voltammetric analysis of the electrolysed solution displayed only a series of peaks from –1.5 to –2.5 V in the cathodic region, and peak **D** during the anodic scan. The latter peak was also observed by direct scan in the anodic potential window. Consequently, the final reduction products are metallic gold, free tppz ligand and Cl^- ions.

On the basis of the voltammetric and macroelectrolysis experiments, the possible reduction pathways for processes **A** and **B** can be described as shown in Scheme 4.

Concluding Remarks

The first gold complex of 2,3,5,6-tetrakis(2-pyridinyl)-pyrazine has been synthesized and spectroscopically characterised. DFT B3PW91 calculations have allowed us to understand some steric and electronic properties of the prepared compound, while electrochemical measurements have allowed us to determine the tetraelectronic nature of the reduction process, which leads to the formation of a stable gold(I)–tppz derivative in solution. Further studies will be carried out in order to obtain new complexes having a gold ion linked by the bridging ligand tppz to another transition metal ion, which could be really interesting from an electrochemical point of view.[3]

Experimental Section

Materials: The salt $K[AuCl_4]\cdot 2H_2O$ was prepared according to a standard procedure starting from metallic Au (99.99%). The ligand 2,3,5,6-tetrakis(2-pyridinyl)pyrazine, the supporting electrolyte tetrabutylammonium perchlorate (TBAP) and benzyltriethylammonium chloride $[BzEt_3N]Cl$ were purchased from Aldrich. Solvents were dried using standard techniques.

Preparation of $[Au_2(OH)_2(tppz)]Cl_4$: This complex was prepared by adding solid 2,3,5,6-tetrakis(2-pyridinyl)pyrazine (0.194 g, 0.5 mmol) to a solution of $K[AuCl_4]\cdot 2H_2O$ (0.414 g, 1.0 mmol) in methanol (25 mL). The reaction mixture was heated to reflux for 12 h. During this time the white, insoluble ligand slowly changed to a bright yellow precipitate, which was filtered after cooling the reaction mixture to room temperature and dried in vacuo. The product was purified by dissolving the solid in the minimum volume of DMF (ca. 6 mL) and filtering the resulting solution. Dropwise addition of diethyl ether (ca. 20 mL) caused the product to precipitate, and this solid was filtered, washed with diethyl ether and dried in vacuo. The complex was obtained in nearly quantitative yield. $C_{24}H_{18}Au_2Cl_4N_6O_2$ (958.18): calcd. C 30.08, H 1.89, Cl 14.80, N 8.77; found C 30.20, H 1.90, Cl 14.85, N 8.80. ^{1}H NMR [$(CD_3)_2SO$, 298 K]: δ = 8.53 (dd, $^3J_{H,H}$ = 5.1, $^4J_{H,H}$ = 1.2 Hz, 4 H, 6-H), 8.26 (dd, $^3J_{H,H}$ = 7.2, $^4J_{H,H}$ = 1.5 Hz, 4 H, 3-H), 8.21 (ddd, $^3J_{H,H}$ = 7.2, $^3J_{H,H}$ = 6.9, $^4J_{H,H}$ = 1.2 Hz, 4 H, 4-H), 7.66 (ddd, $^3J_{H,H}$ = 5.1, $^3J_{H,H}$ = 6.9, $^4J_{H,H}$ = 1.5 Hz, 4 H, 5-H), 6.01 (br. s, 2 H, OH) ppm. $^{13}C\{^1H\}$ NMR [$(CD_3)_2SO$, 298 K]: δ = 153.5, 147.6 (tppz quaternary C atoms), 147.1, 140.2, 125.7, 125.5 ppm (tppz primary C atoms). IR (nujol): $\tilde{\nu}$ = 3412 [ν(O–H)] cm^{-1}. Λ_M (DMF, 298 K) = 159 Ω^{-1} mol^{-1} cm^2.

Physical Measurements: Infrared spectra (4000–400 cm^{-1}, nujol mulls) were recorded with a Perkin–Elmer Spectrum One spectro-

photometer. ^{1}H NMR, ^{1}H COSY and ^{13}C{^{1}H} NMR spectra were obtained with an Avance 300 Bruker spectrometer in $(CD_3)_2SO$ at temperatures between 298 and 338 K. ^{1}H and ^{13}C{^{1}H} NMR spectra are referenced to internal tetramethylsilane. The SwaN-MR and MestRe-C software packages were used to treat the NMR spectroscopic data.[18] Elemental analyses (C, H, Cl, N) were performed by the microanalytical laboratory at the Department of Pharmaceutical Sciences, University of Padua. The conductivity of 10^{-3} M solutions of the complexes in DMF at 25 °C was measured with a Radiometer CDM 83 instrument.

Computational Details: Computational geometry optimisation of the cations $[Au(OH)(terpy)]^{2+}$ and $[Au_2(OH)_2(tppz)]^{4+}$ was performed in vacuo using the restricted DFT B3PW91 method[19,20] without symmetry constraints. The basis sets used were CEP-121G (CEP-31G on the Au atom) (**BS1**),[21] D95V (SDD on the Au atom) (**BS2**) and D95 (LANL2DZ on the Au atom) (**BS3**).[22] Geometry convergence was accelerated using the GDIIS algorithm. All of the resultant stationary points were characterized as true minima (i.e., no imaginary frequencies). Atomic charges were derived from a Mulliken population analysis. All calculations were carried out with computers equipped with Intel Pentium 4 660 processors (Prescott 2M) operating at 3.6 GHz. The software used was Gaussian 98.[23]

Electrochemical Apparatus and Procedure: Voltammetric experiments were performed in an air-tight, three-electrode cell, which was located in a Faraday cage to avoid external noise. Working electrodes of both conventional and micrometric dimensions were employed. The working electrodes of conventional size were either a glassy carbon or a platinum disk of about 3 mm diameter. Preliminary voltammetric tests showed that similar results were obtained whether conventional glassy carbon or platinum disk electrodes were employed as working electrodes, therefore the general voltammetric behaviour of the investigated complex at the conventional glassy carbon electrode is discussed in the text. The microelectrode was a Pt microdisk (25 μm diameter), which was prepared by sealing a 25-μm-diameter wire directly in glass, as reported elsewhere.[16] A platinum spiral was used as counter electrode, and aqueous Ag/AgCl saturated with KCl was used as reference electrode. It was separated from the cell by a salt bridge containing the same solvent and supporting electrolyte solution as used in the cell. All working electrodes were polished mechanically with graded alumina powder (1, 0.3 down to 0.05 μm) on a polishing microcloth. Cyclic voltammetric experiments were performed with a potentiostat/galvanostat PAR 283 A (EG&G) controlled by 270 PAR (EG&G) software using a PC. For experiments with conventional electrodes, positive feedback corrections of the uncompensated resistance (i.r. drop) were performed. Steady-state voltammograms with the microelectrode were recorded at 20 mV s^{-1}. Macroelectrolyses were carried out in an H-shaped cell with the cathodic and anodic compartments separated by a sintered glass disk. As the compound examined displayed comparable voltammetric behaviours on glassy carbon and platinum electrodes, the working electrode used in macroelectrolysis was a large-area platinum gauze, while a platinum spiral served as counter electrode. In controlled-potential electrolyses, an Amel model 552 potentiostat coupled to an Amel model 731 integrator was employed. Unless otherwise stated, voltammetric and coulometric measurements were performed at room temperature using 2 mM $[Au_2(OH)_2(tppz)]Cl_4$ and 0.1 M supporting electrolyte (TBAP) DMF solutions. The cells were degassed with pure nitrogen (99.99%), which was first passed through sulfuric acid solution to remove traces of water and then equilibrated to the vapour pressure of DMF, prior to the measurements.

Acknowledgments

We thank the Ca' Foscari University of Venice for financial support (Ateneo fund 2004).

[1] L. S. Hollis, S. J. Lippard, *J. Am. Chem. Soc.* **1983**, *105*, 4293.
[2] B. Pitteri, G. Marangoni, F. Visentin, T. Bobbo, V. Bertolasi, P. Gilli, *J. Chem. Soc., Dalton Trans.* **1999**, 677.
[3] a) N. Chanda, R. Laye, S. Chakraborty, R. L. Paul, J. C. Jeffery, M. D. Ward, G. K. Lahiri, *J. Chem. Soc., Dalton Trans.* **2002**, 3496; b) N. Chanda, B. Sarkar, J. Fiedler, W. Kaim, G. K. Lahiri, *Dalton Trans.* **2003**, 3550; c) C. M. Hartshorn, N. Daire, V. Tondreau, B. Loeb, T. J. Meyer, P. S. White, *Inorg. Chem.* **1999**, *38*, 3200; d) C. R. Arana, H. D. Abruña, *Inorg. Chem.* **1993**, *32*, 194; e) R. G. Brewer, G. E. Jensen, K. J. Brewer, *Inorg. Chem.* **1994**, *33*, 124; f) L. M. Vogler, K. J. Brewer, *Inorg. Chem.* **1996**, *35*, 818; g) N. Chanda, B. Sarkar, S. Kar, J. Fiedler, W. Kaim, G. K. Lahiri, *Inorg. Chem.* **2004**, *43*, 5128; h) L. M. Vogler, S. W. Jones, G. E. Jensen, R. G. Brewer, K. J. Brewer, *Inorg. Chim. Acta* **1996**, *250*, 155; i) S. W. Jones, L. M. Vrana, K. J. Brewer, *J. Organomet. Chem.* **1998**, *554*, 29; j) R. R. Ruminski, J. L. Kiplinger, *Inorg. Chem.* **1990**, *29*, 4581; k) D. M. Dattelbaum, C. M. Hartshorn, T. J. Meyer, *J. Am. Chem. Soc.* **2002**, *124*, 4938; l) S. Fantacci, F. De Angelis, J. Wang, S. Bernhard, A. Selloni, *J. Am. Chem. Soc.* **2004**, *126*, 9715.
[4] R. Ruminski, J. Kiplinger, T. Cockroft, C. Chase, *Inorg. Chem.* **1989**, *28*, 370.
[5] a) J. Bera, C. S. Campos-Fernández, C. Rodolphe, K. Dunbar, *Chem. Commun.* **2002**, 2536; b) R. R. Ruminski, C. Letner, *Inorg. Chim. Acta* **1989**, *162*, 175; c) J. Lee, L. M. Vrana, E. R. Bullock, K. J. Brewer, *Inorg. Chem.* **1998**, *37*, 3575.
[6] L. M. Vogler, B. Scott, K. J. Brewer, *Inorg. Chem.* **1993**, *32*, 898.
[7] M. Graf, H. Stoeckli-Evans, A. Escuer, R. Vicente, *Inorg. Chim. Acta* **1997**, *257*, 89.
[8] Y. Yamada, Y. Miyashita, K. Fujisawa, K. Okamoto, *Bull. Chem. Soc. Jpn.* **2000**, *73*, 1843.
[9] J. Carranza, C. Brennan, J. Sletten, J. M. Clemente-Juan, F. Lloret, M. Julve, *Inorg. Chem.* **2003**, *42*, 8716.
[10] M. Graf, B. Greaves, H. Stoeckli-Evans, *Inorg. Chim. Acta* **1993**, *204*, 239.
[11] F. Basolo, R. G. Pearson, *Mechanism of Inorganic Reactions*, 2nd ed., Wiley, New York, **1967**.
[12] W. Geary, *Coord. Chem. Rev.* **1971**, *7*, 81.
[13] A. J. Bard, L. R. Faulkner, *Electrochemical Methods*, Wiley, New York, **2001**.
[14] M. I. Montenegro, M. A. Queiros, J. L. Daschbach, *Microelectrodes: Theory and Applications*, NATO ASI Series, **1991**, vol. E197.
[15] J. Tomes, *Collect. Czech. Chem. Commun.* **1937**, *9*, 150.
[16] S. Daniele, M. A. Baldo, M. Corbetta, G. A. Mazzocchin, *J. Electroanal. Chem.* **1994**, *379*, 261.
[17] R. J. Puddephatt, *Comprehensive Coordination Chemistry*, vol. 5 (Ed.: G. Wilkinson), Pergamon, Oxford, **1987**, p. 896 and references cited therein.
[18] a) G. Balacco, *J. Chem. Inf. Comput. Sci.* **1994**, *34*, 1235; b) J. C. Cobas Gómez, F. J. Sardina López, *MestRe-C*, Universidad de Santiago de Compostela, Spain.
[19] R. G. Parr, W. Yang, *Density-Functional Theory of Atoms and Molecules*, Oxford University Press, Oxford, **1989**.
[20] a) A. D. Becke, *J. Chem. Phys.* **1993**, *98*, 5648; b) K. Burke, J. P. Perdew, Y. Wang, in *Electronic Density Functional Theory: Recent Progress and New Directions* (Eds.: J. F. Dobson, G. Vignale, M. P. Das), Plenum, New York, **1998**.
[21] T. R. Cundari, W. J. Stevens, *J. Chem. Phys.* **1993**, *98*, 5555.
[22] T. H. Dunning Jr., P. J. Hay, *Modern Theoretical Chemistry*, vol. 3 (Ed.: H. F. Schafter), Plenum, New York, **1976**.
[23] a) M. J. Frisch, G. W. Trucks, H. B. Schlegel, G. E. Scuseria, M. A. Robb, J. R. Cheeseman, V. G. Zakrzewski, J. A. Montgomery Jr, R. E. Stratmann, J. C. Burant, S. Dapprich, J. M.

Millam, A. D. Daniels, K. N. Kudin, M. C. Strain, O. Farkas, J. Tomasi, V. Barone, M. Cossi, R. Cammi, B. Mennucci, C. Pomelli, C. Adamo, S. Clifford, J. Ochterski, G. A. Petersson, P. Y. Ayala, Q. Cui, K. Morokuma, D. K. Malick, A. D. Rabuck, K. Raghavachari, J. B. Foresman, J. Cioslowski, J. V. Ortiz, A. G. Baboul, B. B. Stefanov, G. Liu, A. Liashenko, P. Piskorz, I. Komaromi, R. Gomperts, R. L. Martin, D. J. Fox, T. Keith, M. A. Al-Laham, C. Y. Peng, A. Nanayakkara, M. Challacombe, P. M. W. Gill, B. Johnson, W. Chen, M. W. Wong, J. L. Andres, C. Gonzalez, M. Head-Gordon, E. S. Replogle, J. A. Pople, *Gaussian 98*, Gaussian, Inc., Pittsburgh PA, **1998**. We thank Dr. A. Zambon for the use of his software package.

Received: April 26, 2006
Published Online: July 21, 2006

